Applied Ocean Research 67 (2017) 248–262

Contents lists available at ScienceDirect

Applied Ocean Research

journal homepage: www.elsevier.com/locate/apor

Assessment of URANS surface effect ship models for calm water and head waves

Shanti Bhushan [a], Maysam Mousaviraad [b,1], Frederick Stern [b,*]

[a] Department of Mechanical Engineering, Mississippi State University, Starkville, MS, USA
[b] IIHR-HydroScience and Engineering, The University of Iowa, Iowa City, IA, USA

ARTICLE INFO

Article history:
Received 29 August 2016
Received in revised form 23 July 2017
Accepted 24 July 2017

ABSTRACT

Surface effect ship (SES) air cushion and seal models are implemented in an URANS hydrodynamics solver. The air cushion is modeled either as a prescribed pressure patch, or as a compressible isothermal/adiabatic ideal stagnant air with fan and leakage flows. The seals are either discretized as hinged bodies or modeled as 2D planing surfaces with hydrodynamic interaction. Verification and validation studies are performed using T-Craft experimental data for calm water resistance, sinkage and trim at Froude number (Fr) = 0.1–0.6; impulsive heave and pitch decay at Fr = 0; and wave-induced resistance and motion predictions in head waves at Fr = 0 and 0.6. The compressible air cushion model with fan and leakage flows perform better than those without the fan and leakage flows and the prescribed pressure patch model. The hinged seal model performs better than the 2D planing surface model, but is computationally expensive for time accurate simulations. Therefore, the 2D planing surface model is used for the validation studies. SES simulations on grids with 5.3 M cells show grid verification intervals of 6%, which are comparable to those reported for displacement and semi-planing hull studies on similar grid sizes. On an average calm water and impulsive motion predictions compare within 8.5% of the experimental data, and wave-induced motion predictions show somewhat larger error of 13.5%. The errors levels are mostly comparable to those for displacement and semi-planing and planing hulls. The study identifies that most critical advancement needed for SES simulations is the seal modeling including fluid structure interaction.

1. Introduction

Potential flow (PF) and Unsteady Reynolds Averaged Navier Stokes (URANS) predictions for air cushion vehicles (ACV)/surface-effect ships (SES) requires additional modeling for the air cushion and seals, including their interactions with hydrodynamics. Air cushion modeling is complex as it involves compressible flow with fan inflow and leakage from underneath the seals, and variable cushion volume due to ship motions. Seal modeling is very complex due to their geometry, flexibility and air inflation.

Doctors [1,2] developed an ACV model, wherein hydrodynamics was modeled using a linearized free-surface PF method and air cushion pressure was prescribed on the free-surface. The model was used for straight ahead and yawed ACV air cushion wave resistance ($C_{\zeta c}$) predictions, and results were compared with experimental data and URANS predictions [3,4]. The URANS predictions used a single-phase level-set solver for hydrodynamics with prescribed air cushion pressure. In both the PF and URANS studies, $C_{\zeta c}$ was estimated from the slope of the wave elevation in the air cushion. Both the URANS and PF predictions compared within 7%D of the experimental data (D) for Fr > 0.5; however, URANS performed better than PF at lower Fr. In addition, PF failed to predict the effect of shallow water and high air cushion pressure effects. The model was extended for SES, wherein the catamarans were represented by source singularities along the center-line, and air cushion was prescribed on the free-surface. The model was applied for JJMA SES resistance predictions [5,6]. The predictions were validated using experimental data and compared with URANS [7]. The hull and air cushion pressure wave resistances were computed from the integral of resultant far-field wave elevation. The hull frictional resistance was computed using the predicted dynamic wetted area, and ITTC correlation. The bow seal resistances were computed separately from the finite pressure element solutions of the flow under a 2D planing surface over the free-surface. Both the PF and URANS

* Corresponding author.
E-mail address: Frederick-stern@uiowa.edu (F. Stern).
[1] Current Affiliation: Department of Mechanical Engineering, University of Wyoming, Laramie, Wyoming, USA.

http://dx.doi.org/10.1016/j.apor.2017.07.013
0141-1187/

[7] solvers showed similar trends for the resistance predictions. The PF resistance predictions compared within 14%D of the experimental data, slightly better than URANS which showed error of 18.7%D. The primary difference between the two solvers was reported to be the transom wave elevation predictions.

Milewski et al. [8,9] developed ACV/SES model by coupling a spline-based boundary element model for hydrodynamics, wherein the hull was represented by Rankin sources; air cushion was modeled as a compressible fluid with fan and leakage flows; and the seals were modeled as a lumped-mass hinged body which rotated at the deck pivot due to the air cushion pressure and hydrodynamic forces and moments. The model was applied for the prediction of LCAC ACV calm water sinkage and trim, and pitch and heave motions in regular head waves and in sea-states SS3 and SS4; Transformable-craft (T-Craft) SES seakeeping in regular head waves and in SS4 at $Fr = 0$; and seakeeping response of T-Craft when moving alongside a cargo container. Heave force and pitch moment were computed by adding the hydrodynamic forces and moment acting on the hull wetted surface, and those due to air cushion pressure over the dry surface of air cushion (i.e., excluding the free-surface). For the LCAC simulations, the results were in good agreement with the experimental data. However, T-Craft pitch and heave prediction errors were large, especially for longer wavelengths. For the ship-ship simulations, the T-Craft heave and pitch response showed significantly large errors, whereas the cargo container motions were predicted reasonably well.

Bandas and Falzarano [10] and Lee and Newman [11] used low-order linear PF solver for hydrodynamics; air cushion was modeled as a compressible fluid without fan and leakage flows; and seals were neglected. The model was validated for T-Craft seakeeping in head and bow waves. The forces and moments were computed from the pressure distribution on the hull wetted surface and air cushion pressure acting on the dry air cushion surface. The study reported that the compressible fluid air cushion model predicts the ship motions better than the prescribed pressure model. Overall, the trends in the 1st harmonics of the ship motions were similar to the experimental data, however the errors were large both for longer and shorter wavelengths.

Mouravieff [12] and Donnelly and Neu [13] used a two-phase URANS solver for hydrodynamics; compressible ideal gas solution including fan and leakage flows for the air cushion flow; and discretized rigid seal model. The solver were applied for SES XR–100 B and T-Craft resistance and limited seakeeping predictions. The forces and moments were computed by adding the integral of the pressure and viscous stresses over the hull and the seal wetted areas, and those over the superstructure. Resistance predictions were 40–100% higher compared to the experiments, and the seakeeping simulations showed significant plowing through the water with high-amplitude breaking bow waves. Donnelly and Neu [13] shortened the seals to be above the waterline at static conditions to avoid plowing through the water, which resulted in resistance and seakeeping response within 10% of the experiments, but caused excessive leakage. The study emphasized the need for dynamic, flexible seal modeling.

Maki et al. [7] used a single-phase level-set URANS solver for hydrodynamics; prescribed air cushion pressure; and 2D planing surface seal model without hydrodynamic interaction [1]. The model was applied for JJMA SES resistance predictions. Resistance was obtained by linearly adding the hull resistance, seal resistance, air resistance over the super structure, and the resistance due to air cushion pressure acting over the air cushion dry surface. The hull resistance was obtained from the integral of pressure and viscous stresses over hull wetted surface. The seal resistance was estimated from the 2D planing surface model. The air resistance was estimated using bluff body drag coefficient and superstructure projected area. Resistance due to the air cushion pressure on the dry air cushion area was estimated assuming equilibrium condition in the air cushion. The URANS resistance predictions showed somewhat higher errors than PF predictions, as discussed above.

The review of literature shows that URANS performs better than PF for the non-linear interaction between the air cushion pressure and the hull. The air cushion models based on compressible fluid with fan and leakage flows perform better than the prescribed air cushion pressure models, and are reasonably accurate for wave-induced motion predictions. Different seal models have been used, such as discretized rigid, hinged bodies, or 2D planing surface; however, there is no clear consensus regarding the best seal modeling, and the interaction of the seals with hydrodynamics has been mostly neglected. Comprehensive validation studies are lacking as studies have focused primarily on wave-induced motions, and limited studies have included detailed validation for resistance. Studies agree that SES resistance (C_T) should be computed from the integration of: pressure (C_p) and viscous stresses (C_f) over the hull wetted surface; pressure and viscous stresses over the seal wetted surface (C_s); air pressure and viscous stresses over the super-structure (C_A), and air cushion pressure over the air cushion dry surface (C_{ac}). A similar approach should be used for the calculation of other forces and moments. In all the studies discussed above, C_p and C_f have been computed from hull integration. C_s has been either computed from the hull integration for discretized seals, or estimated from 2D planing surface model. C_A have been obtained from the surface integral for two-phase simulations, whereas estimated using bluff body drag coefficient for single-phase simulations. The studies show the most variation for the C_{ac} calculations. Studies [12,13] neglected their contribution, studies [9–11] used direct surface integration, whereas study [7] assumed an equilibrium condition for the air cushion and its boundaries, thus estimating $C_{ac} = C_{\zeta c}$.

The objective of this study is to extend the previous URANS ACV model [3] for SES capability by implementing compressible air cushion and seal models. Guided by the above studies, the air cushion is modeled as a compressible isothermal/adiabatic ideal stagnant air with fan and leakage flows. The seals are either discretized as rigid and hinged bodies, or modeled as 2D planing surfaces with hydrodynamic interaction. A detailed assessment of the models is performed based on verification and validation studies using T-Craft experimental data for calm water resistance, sinkage and trim at $Fr = 0.1$ to 0.6; impulsive heave and pitch at $Fr = 0$; and resistance and motions in regular head waves at $Fr = 0$ and 0.6. To investigate the validity of equilibrium assumption for the air cushion, as used by Maki et al. [7] for C_{ac} calculations, the T-Craft resistance components are analyzed, and compared with JJMA results.

2. URANS SES models

2.1. Hydrodynamics

CFDShip-Iowa V4.5 solves the URANS/DES equations for the water phase in absolute inertial earth-fixed coordinates [14]. The turbulent eddy viscosity is obtained from the solution of the two-equation blended k-ω/k-ε turbulence model. The location of the free surface is given by a 'zero' value of the level-set function, which is advected as a material surface. Negligible shear stress is assumed in the air phase, which provides the pressure-jump condition at the free surface. The governing equations are discretized using finite-difference schemes on body-fitted curvilinear grids. The convection and diffusion terms are discretized using a second-order scheme. The pressure Poisson equation is solved to satisfy continuity using a projection algorithm. Time marching is performed using a second-order backward-difference scheme. Six degree-of-freedom (6DoF) motions are solved implicitly using dynamic multi-block grids with overset grid interpolation. Message Passing Interface (MPI) based domain decomposition is used for parallel simulation. The solver has undergone extensive verification and validation for numerous applications [15].

2.2. Air cushion

Fig. 1(a) shows the T-Craft geometry, including catamarans, forward and aft air cushions, and bow, stern and transverse seals [16]. The forward (f) and aft (a) air cushion pressures P_{Qi} ($i=f$ or a) are either prescribed using hydrostatic values P_{0i} (provided in Table 1), or computed assuming compressible isothermal/adiabatic ideal stagnant air with or without fan and leakage flows. P_{Qi} at time step $(t+1)$ is determined from the previous time step (t):

$$P_{Qi}(t+1) = P_{Qi}(t) + \left[Q_{fi} - Q_{li} - \frac{\partial V_i(t)}{\partial t}\right] \frac{\gamma[P_{Qi}(t)+P_A]}{V_i(t)} \Delta t \quad (1)$$

where, the heat capacity ratio $\gamma=7/5$. Q_{fi} and Q_{li} are the fan and leakage flow rates, respectively, as shown in Fig. 1(b). $V_i(t)$ is the instantaneous cushion volume, which depends on the SES motions and air cushion wave elevation, and may not be equal to the hydrostatic volume V_{0i}. The initial condition for the air cushion pressure equations is the hydrostatic condition $P_{Qi}(t=0)=P_{0i}$. Air cushion pressures computed without fan and leakage flows, i.e., $Q_{fi}=0$ and $Q_{li}=0$, are designated as P_i. Note that for catamaran operation, P_{Qi} are specified as atmospheric pressure (P_A).

The fan inflow is determined by the fan curve shown in Fig. 1(c) such that Q_{fi} is zero for $P_{Qi}=P_{0i}$ and maximum for $P_{Qi}=P_A$. The fan curve was validated for the air cushion pressurization simulations, i.e., prediction of forward and aft air cushion pressures and heave as the cushion is pressurized from an initial $P_{Qi}=P_A$. As shown in Fig. 1(d), the air cushion pressures and heave predictions compare within 6%D of the experimental data, thus validating the fan curve implementation.

Leakage from the forward and aft air cushions occurs through the gaps (or leakage area is designated as A_i) underneath the bow and stern seals, respectively. Leakage also occurs between the forward and aft air cushions underneath the transverse seals, which are neglected. The leakage flow rate is obtained using Bernoulli's equation assuming spanwise uniformity:

$$Q_{li} = C_d A_i \sqrt{\frac{2\left\{P_{Qi}(t) - P_A\right\}}{\rho_A}} \quad (2)$$

where, ρ_A is the density of air. Faltinsen [17] recommends discharge coefficient $C_d \approx 0.6$ and 1.0 for bow and stern seal leakage, respectively.

2.3. Seals

The bow seals are flexible fingers, which deflect and drag downstream at the free surface. The stern seal is a flexible bag consisting of multiple pressured lobes, and is open against the side hulls. They are pressurized at a higher pressure than the air cushion, and typically drag on the water surface. The seals are designed not to leak at hydrostatic condition. However, they invariably leak when subject to ship motions, especially the stern seals. The transverse seal separates the forward and aft cushions, and has nearly equal pressures pushing on it from opposite sides. Thus, the pressure drag on the transverse seal surface is expected to be small. A similar conclusion was drawn by Day et al. [18], wherein it was reported that the multiple cushion partitions do not significantly affect the SES resistance. Thus in this study, the transverse seals are neglected and only the bow and stern seals are modeled. The seal models considered herein include: discretized rigid or hinged bow and stern seals; and bow seal approximated as a 2D planing surface with hydrodynamic interaction.

Rigid (undeflecting) seals are included as part of the hull geometry, and move with the catamaran hull. Hinged seals pitch and heave rigidly with the hull, but in addition roll motion in the Y-axis pivoted at the intersection of the seal top and wet deck. To allow the hinged seal roll motion, the hull and seals were discretized as separate bodies, with a small gap.

In the 2D planing surface seal model, same shape and wetted length l_s is assumed along the beam (B_c). As shown in Fig. 1(e), the seal deflection is assumed as a cubic profile between the beam averaged wave elevation at the bow (ζ_s) and the seal trailing edge immersion length (δ_S). The wetted seal length (l_s) is computed from the undeflected seal immersion height (H_s) and seal slope ($\theta_0=51^\circ$). The unknowns δ_S, seal resistance (R_{BS}) and seal lift (L_{BS}) are coupled, and are evaluated using Newton-Raphson iteration of the PF finite pressure elements results.[2] Following that, 2D planing seal pressure (P_{BS}) variation along l_s is calculated from a look-up table (obtained from PF results). The potential flow predicts a sharp increase in the pressure coefficient near the seal leading edge, as the pressure matrix results in a singularity at $x/l_s=1$ [1], which can lead to numerical instability. Thus, the peak pressure coefficient (based on the seal length l_s) is clipped such that the seal leading edge pressure is lower than the fluid stagnation pressure.

The 2D planing surface model is not used to model the stern seal in the current simulations; since, the stern seal is designed to just touch the free-surface in calm water conditions, and is usually out of the water and leaks during typical operation [2,19]. However, it may affect the flow for lower Fr [18], and should be included in future research.

2.4. Interaction of air cushion and seal models with hydrodynamics

The air cushion and seal models interact with the hydrodynamics through boundary conditions, and forces and moments. The air cushion and seal resistance (R), heave force (Y) and yaw moment (N) are added to the respective hydrodynamic components. The net heave force and yaw moment are used in the 6DoF solver for heave/sinkage and pitch/trim predictions.

The air cushion pressures P_{Qi} are applied on the free-surface as a boundary condition, as shown in Fig. 2. The pressure patch location is determined based on the SES motions. P_{Qi} acts on the dry air cushion surface (A_{ac}), including the bow and stern seals and wet-deck, resulting in air cushion resistance R_{ac}, heave force Y_{ac} and pitch moment N_{ac}. Assuming that the seals just touch the free-surface, the integral over A_{ac} is equivalent to the multiplication of P_{Qi} with the net projected area in the streamwise normal plane.

$$R_{ac} = \int_{A_{ac}} P_{Qi} dA_x = \left[P_{Qf}L_f + P_{Qa}L_a\right] B_c \sin(\tau) \quad (3)$$

where, L_f and L_a are the forward and aft cushion lengths, respectively, and τ is the trim angle (or pitch). Heave force Y_{ac} is computed as:

$$Y_{ac} = \int_{L_c B_c} \left(P_{Qi} - P_{0i}\right) dxdy \quad (4)$$

[2] Potential flow results were provided by Prof. Lawrence J. Doctors (The University of New South Wales, Sydney, Australia) for flat, parabolic and cubic planing surfaces. The cubic planing surface is used in this study as they provided the most accurate T-Craft resistance predictions when compared to the experiment.

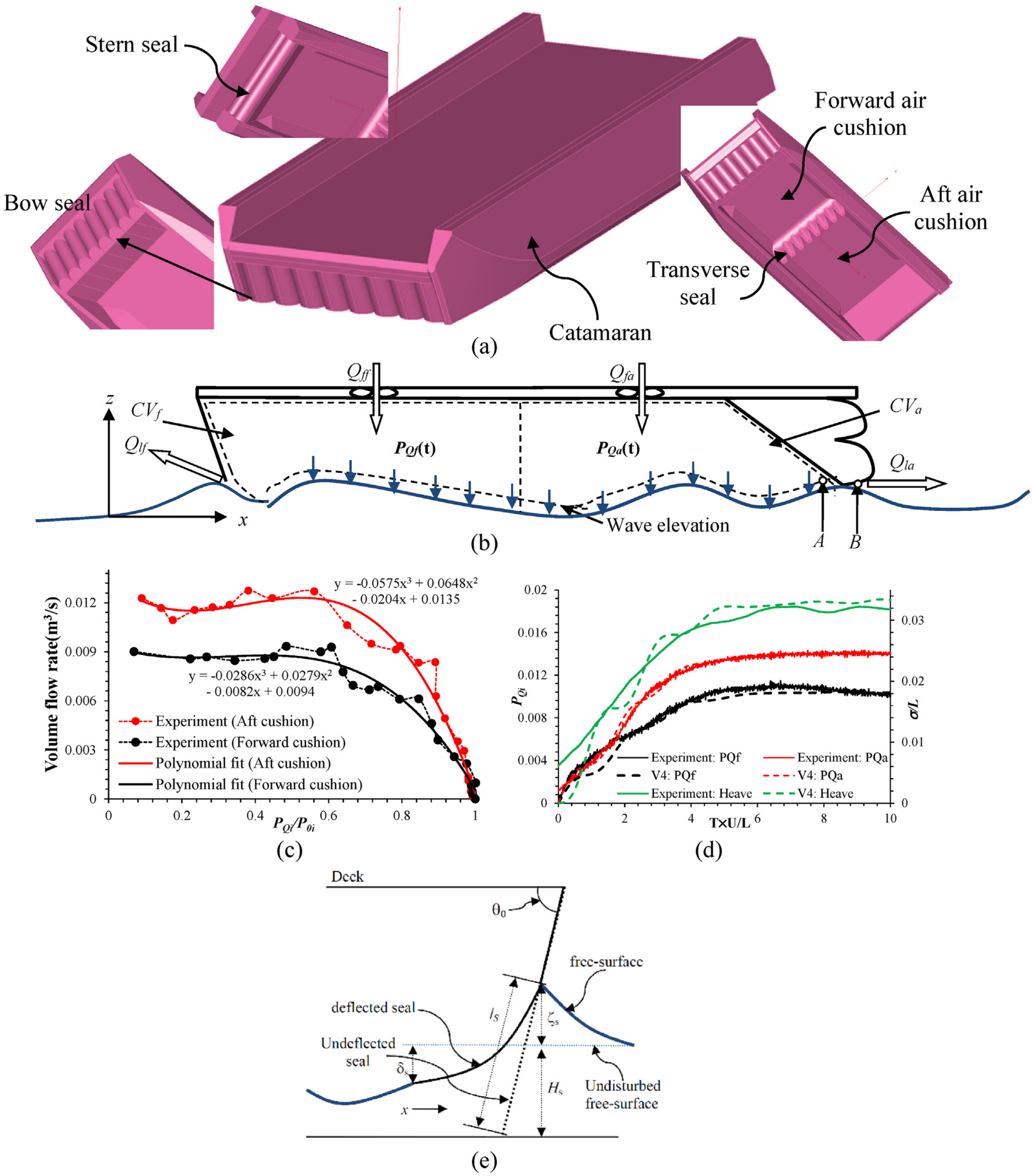

Fig. 1. (a) A view of the T-Craft geometry and seals. (b) Typical SES cross-section showing forward and aft air cushion pressure (P_{Qi}), control volume (CV_i), including fan (Q_{fi}) and leakage (Q_{fa}) flows. Subscript i is replaced by f and a for forward and aft air cushions, respectively. (c) Forward and aft air cushion fan curve derived from 3rd order polynomial curve fit of the experimental data [16]. (d) URANS air cushion pressure and heave predictions for the air cushion pressurization study are compared with experimental data. (e) Schematic diagram showing the key components of the 2D planing surface model for the bow seal [1].

N_{ac} is calculated from the moment of the air cushion pressure force acting on the net projected area in the free-surface normal plane as:

$$N_{ac} = ½\left[P_{Qf}{L_f}^2 - P_{Qa}{L_a}^2\right] B_c cos(\tau) \quad (5)$$

The rigid and hinged seal models interact with the hydrodynamics through no-slip wall boundary condition. The hinged seal rotation (ϕ) is governed by the hydrodynamics moment M_H created by the fluid pressure and viscous stress distribution on the wetted seal surface, and the restoring moment due to P_{Qi} acting on the seal surface inside the air cushion:

$$k\frac{d^2\phi}{dt^2} = M_H - \frac{1}{2}{H_s}^2 B_c P_{Qi} \quad (6)$$

where, H_s is the projected height of the wetted seal in the stream-wise normal direction, and k is the moment of inertia which dictates

Table 1
Particulars of model- and full-scale T-Craft and full-scale JJMA.

Parameter (Unit)	T-Craft			JJMA
	Model-scale	Full-scale	Non-dimensional	
Vehicle length L *(m)*	2.52	76.35	1 L	80.14m
Vehicle beam B *(m)*	0.7366	22.25	0.29 L	0.306 L
Cushion length L_c *(m)*	2.23	67.14	0.885 L	0.898L
Cushion width B_c *(m)*	0.546	16.50	0.216 L	0.218L
Draft T catamaran operation *(m)*	0.13	3.93	0.051 L	–
Draft T SES operation *(m)*	0.044	1.33	0.0175 L	0.0172L
Static cushion height h_0 *(m)*	0.088	2.66	0.0347 L	–
Vertical center of gravity below deck *(m)*	0.00635	0.19	0.00252 L	–
Catamaran area catamaran operation A_w (m^2)	0.4752	433.7	0.0744 L^2	–
Catamaran area SES operation A_w (m^2)	0.3181	290.36	0.0501 L^2	–
Radius of gyration for pitch r_{yy} (m)	0.717	21.71	0.2844 L	–
Radius of gyration for roll r_{zz} (m)	1.07	32.26	0.4225 L	–
Volume of fresh water displacement (m^3)	0.055163	1519.5	0.00345 L^3	–
Catamaran buoyancy SES operation *(N)*	540.0675	14.875×10^6		–
Block coefficient C_B catamaran operation ($_{catamaran}$[a]$/LBT$)	0.229			–
Block coefficient C_B SES operation ($_{catamaran}/LBT$)	0.256			–
Forward air cushion pressure P_{0f} (N/m^2)	220.61	6664.63	$P_{Qf}/\rho g L_c = 0.0101$	$P_c/\rho g L_c =$ *0.0009–0.0189*
Aft air cushion pressure P_{0a} (N/m^2)	296.442	8955.51	$P_{Qa}/\rho g L_c = 0.0136$	
Vehicle mass (M)	55.26 kg	1,528.86 Ton	–	2239 Ton

[a] $_{catamaran}$ is the volume of catamarans submerged in water.

the convergence of the solution and is chosen through numerical experiments for stability.

For 2D planing surface bow seal model, P_{BS} is applied as a pressure patch on the free-surface. The patch location is determined based on the SES motions. The seal resistance R_{BS} and heave force $Y_{BS} = L_f$ are obtained from the 2D planing seal model as discussed above. The pitch moment N_{BS} is computed as:

$$N_{BS} = L_f X_{BS} \tag{7}$$

where X_{BS} is the streamwise distance of the bow seal pressure patch from the SES center of rotation.

3. T-Craft experimental data, and simulation setup and conditions

3.1. Experimental data and conditions

Naval Sea System Command Carderock Division built a 1/30.21 T-Craft model with hull length (L) of 2.52 m to procure resistance, sinkage and trim; impulsive motion; and wave-induced motion data in deep-water [16]. The particulars of the T-Craft model are provided in Table 1 for static conditions in calm water. During operation, catamaran buoyancy supports 63% of the vehicle weight, and air cushion pressure the rest.

As summarized in Table 2, experimental data used in this study are: (1) time history of air cushion pressures and heave as the air cushion is pressurized from catamaran mode to SES mode; (2) calm-water resistance, sinkage and trim for Froude number (Fr) = 0.08, 0.2, 0.4 and 0.6; (3) time history of motions and cushion pressures for impulsive pitch and heave decay in calm water at $Fr = 0$; (4) time history of pitch and heave motions, and air cushion pressures in regular head ($\mu = 0^\circ$) waves with wavelengths $\lambda/L = 0.66$–5.0 and wave steepness (Ak) of 0.05 at $Fr = 0$; and (5) time history of resistance, pitch and heave motions, and air cushion pressures in regular head waves with $\lambda/L = 0.98$, 1.25 and 1.63 and $Ak = 0.05$ at $Fr = 0.6$.

The experimental data also included: time history of motions and cushion pressures for impulsive roll decay in calm water at $Fr = 0$; time history of pitch, heave and roll motions, and air cushion pressures in regular bow $\mu = 20^\circ$ and beam $\mu = 90^\circ$ waves with wavelengths $\lambda/L = 0.66$–5.0 at $Fr = 0$; and time history of pitch, heave and roll motions, and air cushion pressures in SS4 with modal wave period of $\tau_p = 8.2$ s for headings $\mu = 0^\circ$, 20°, 75° and 90° at $Fr = 0$. In addition, wave-induced motion experiments were performed for multi-body case, i.e., T-Craft alongside or connected to a cargo container or mobile landing platform.

Experiments provide an extensive dataset for validation; however, there are significant limitations for CFD validation due to lack of experimental uncertainty (U_D) estimates and documentation of wave-induced motion measurement systems. The wave maker used for the experiments is known to produce wave group representations of the ideal regular wave conditions. Experiments also involve additional complexity due to air cushion and seals, similar to the numerical modeling. Nonetheless, available experimental data are useful in assessing URANS prediction capability, and especially in evaluating the performance of air cushion and seal modeling to guide future research priorities.

3.2. Simulation setup and conditions

The T-Craft geometry is simplified for the ease of grid generation. The simplifications include: modification to the deck, removal of the transverse seal, and replacement of the bow seal fingers with a flat surface and stern seal lobes with a curved surface for the rigid and hinged seal simulations. No significant changes are expected due to the deck and stern-seal modifications as they are expected to be in the air. All the simulations are performed using half domain grids with symmetry at Y = 0 plane. The half domain grid extends from X = [−1.5, 5]L, Y = [0,2]L and Z = [−4,1]L. The large negative Z-extent (which is in the water phase) is used to satisfy the deep water conditions.

As shown in Table 2, the simulations with rigid and hinged seal were performed using grids consisting of 7.4 M and 6.2 M total cells, respectively. The grid verification study is performed using P_{Qi} and 2D planing surface seal model with five systematically refined grids consisting of 1.84 M (grid #5), 3.09 M (grid #4), 5.2 M (grid #3), 8.75 M (grid #2) and 14.71 M (grid #1) cells. Two systematic grid studies are performed, first with grid refinement ratio of $r_G = 2^{1/4}$ for grid# 1, 2 and 3, and second with $r_G = 2^{1/2}$ for grid# 1, 3 and 5. Considering the reasonable grid uncertainties (as discussed below) and computational cost, grid #3 is used for the validation study. As shown in Fig. 2, no-slip wall boundary conditions are specified on the body fitted hull grids, whereas inflow, outlet and far-field boundary conditions are specified on the Cartesian background grid. A refinement block is used for proper overset grid interpolation close to the hull.

Table 2
Summary of T-Craft validation cases, simulation conditions, models and grids, validation variables and objectives.

Simulation Condition					Models	Grid(s)	Experimental data	Objective
Case #	Case		Re	Fr				
1	Air cushion pressurization		0	0	P_{Qi}; No Seals	5.2M	Time history of P_{Qf}, P_{Qa} and heave	√ Obtain T-Craft fan curve
2	Calm water resistance, sinkage and trim	1.0–7.3 × 10^6	0.1–0.6	$P_{A,}$ P_{0i}, P_i, P_{Qi}; No, Rigid, Hinged, and 2D planing surface seal	Rigid: 7.4 M; Hinged: 6.2 M; Planning: 1.84 M, 3.09 M, 5.20 M, 8.75 M, 14.71M	C_T, sinkage, trim and P_{Qi} for Fr = 0.08, 0.2, 0.4 and 0.6	√ Verification for C_T, sinkage, trim, P_{Qi}, and wave elevation	
		√ Validation of air cushion and seal models √ Validation of URANS SES model for resistance, sinkage and trim predictions						
3	Impulse response	Heave	0	0	$P_{A,}$ P_{0i}, P_i, P_{Qi}; 2D planing surface seal	5.2 M	Time history of pitch, heave and P_{Qi}	√ Validation of air cushion models √ Validation URANS SES model for natural frequency, motion and air cushion pressure predictions
		Pitch				5.2 M		
4	Wave-induced motions in regular head waves, Ak = 0.05	λ/L = 5, 3.19, 2.22, 1.63, 1.25, 0.985 and 0.8	0	0	P_{Qi}; 2D planing surface seal	5.2 M	Time history of pitch, heave and P_{Qi}.	√ Grid verification for resistance, pitch and heave for Fr = 0.6
5		λ/L = 3.19, 2.22, 1.63, 1.25, 0.985 and 0.8	7.3 × 10^6	0.6		5.2 M	Time history of pitch, heave, P_{Qi}, and C_T.	√ Validation of URANS SES model for 0th and 1st harmonics of resistance, motions and P_{Qi}; phases of pitch and heave; and added resistance

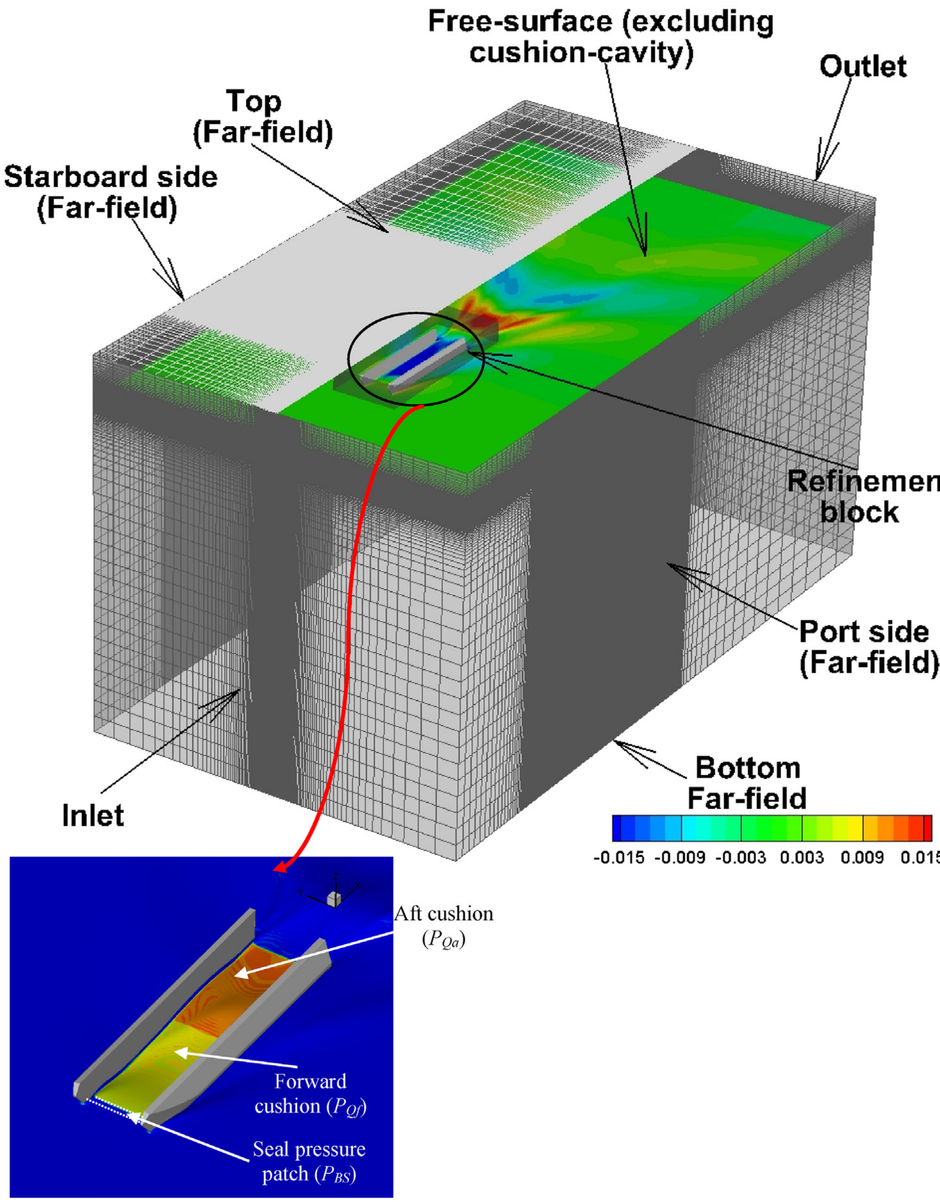

Fig. 2. Domain, grids and boundary conditions for T-Craft simulations. The inset figure shows the T-Craft model, wherein Catamarans are resolved, and pressure patch is applied for the air cushion pressure (P_{Qf} and P_{Qa}) and 2D planning surface bow seal (P_{BS}).

The URANS simulations performed in this study are summarized in Table 2, which includes: (1) air cushion pressurization to validate air cushion fan model at $Fr = 0$; (2) resistance, sinkage and trim at $Fr = 0.1$ to 0.6, which correspond to Reynolds number (Re) = 10^6 to 7.3×10^6 (where Re is based on L and inflow velocity U_0), including grid verification for $Fr = 0.2$ and 0.6; (3) impulsive heave and pitch decay at $Fr = 0$; and resistance and wave-induced motions in regular head waves for (4) $\lambda/L = 0.8$–5.0 at $Fr = 0$, and (5) $\lambda/L = 0.8$–3.19 at $Fr = 0.6$ and Re 7.3×10^6. For the wave simulations, validation is performed for the 0th harmonic (denoted by subscript 0), 1st harmonics (denoted by subscript 1) and phases of resistance, heave (z) and pitch (θ).

4. Verification

Verification studies follow [20,21] to estimate iterative (U_I) and grid convergence (U_G) uncertainties, as summarized in Table 3. $U_I < 0.4\%S_1$, where S_1 is the solution on the finest grid, for both calm water and wave simulations. Thus, the iterative convergence is acceptable. The calm water solutions show poor grid convergence for the coarser grid triplets, whereas show mostly monotonic convergence the finer grid triplets. Wave solutions show monotonic convergence for both the grid triplets. The averaged ratio of numerical and theoretical order of accuracy varies from $P_G = 0.6$ to 3. For calm water, $U_G = 3\%S_1$, $5.4\%S_1$, $11.5\%S_1$ and $9.5\%S_1$ for C_T, sinkage, trim and wave elevation, respectively. For wave simulations, $U_G = 4.6\%S_1$, $4\%S_1$ and $2.3\%S_1$ for C_T, motions and phases, respectively.

Overall, the iterative uncertainties are small, U_G for motions and wave elevations are larger than that for resistance, and U_G values are higher for $Fr = 0.2$ than those for $Fr = 0.6$. It is well accepted that CFD simulations should use at least second order accurate numerical methods, as used in the current study. A previous study [22] has demonstrated that the solver achieves the theoretical order of accuracy for idealized problems. However for complex applications, such as the one considered here, the estimated numerical order of accuracy of the simulations is expected to deviate from the theoretical value. This is due to errors expected from other factors, such as modeling and numerical methods, domain size, boundary conditions, and grid design to name a few. The purpose of the verification is to assess the numerical uncertainty for the applications due to grid resolution. The grid uncertainties are reasonable considering the complexity of SES modeling, and are comparable to those reported by displacement [23] and semi-planing hulls [24] studies on similar size grids, as summarized in Table 4. Therefore, current grids are deemed satisfactory for validation studies.

5. Validation for calm water resistance, sinkage and trim

The resistance encountered by a body in contact with a fluid is evaluated using the integral of the pressure and shear stresses over its surface in contact with the fluid. A SES interacts with the water through catamarans and seals, the air in the superstructure, and the air cushion pressure. The total SES resistance is:

$$C_T = C_p + C_f + C_s + C_A + C_{ac} \tag{8}$$

Note that the resistance coefficients are obtained by non-dimensionalizing drag by the U_0 and wetted hull area (A_w). The hydrodynamic resistance coefficients, C_p and C_f are computed from the pressure and viscous stress distribution over the wetted hull surfaces. C_s is estimated from the 2D planing seal model as discussed in Section 2. Air drag over the super structure C_A is estimated following [6] as below:

$$C_A = \frac{\rho_A A_f}{\rho A_W} C_D \tag{9}$$

where, ρ_A is the density of air and A_f is the frontal area of the superstructure, and a drag coefficient of $C_D = 0.826$ is used following [6]. C_{ac} is calculated from the integration of air cushion pressure over the dry air cushion surface, as shown in Eq. (3). All the resistance coefficients, except for C_A, are computed during run-time. C_A is added aposteriori to the converged solution.

Table 5 and Fig. 3 summarize the calm water resistance, sinkage and trim results. Preliminary studies compared no seal, rigid, hinged and 2D planing surface seal models using $P_{Qi} = P_{0i}$, and compared P_{Qi}, P_i and P_{0i} air cushion models using 2D planing surface seal model. The errors from smallest to largest are obtained using hinged, 2D planing surface, rigid and no seal models. Among the air cushion models, P_{Qi} is the best followed by P_i and P_{0i}. Therefore, subsequent validation studies are carried out mostly using the P_{Qi} and the 2D planing surface seal models.

As shown in Fig. 3(a), experimental data for C_T is sparse with values for only four Fr, whereas URANS has values for several Fr. Gross trends in both the experiment and URANS are similar. Both show max C_T at low Fr followed by decreasing values with increasing Fr. URANS also indicates oscillations with humps at $Fr = 0.3$ and 0.44. The humps are due to peaks and troughs in the air cushion wave elevation (as shown in Fig. 3e), which result in humps and hollows in the air cushion wave resistance [3]. On an average, the C_T predictions agree within 3%D of the experimental data; however, shows large 14%D error for the two lower Fr. As shown in Fig. 3(b), the gross trends for sinkage are similar to the data, but URANS shows oscillations at C_T humps. The sinkage and trim predictions show large average errors of 32%D and 62%D, respectively. The large errors are due to small sinkage and trim values, where the maximum sinkage is about 11% of the draft and trim is 1°. Errors expressed using dynamic range (DR) of the motions result in a reasonable average error of 12%DR. Fig. 3(c) and (d) shows errors of 2%D and 8.3%D for the forward and aft air cushion pressures, respectively. The relatively larger error for the aft air cushion pressure could be due to the negligence of the stern seal effects.

The T-Craft resistance and its components are compared with those of JJMA [7] in Fig. 4. As summarized in Table 1, both T-Craft and JJMA have similar air cushion dimensions. As shown in Fig. 4(a),

Table 3
Verification study for the predictions of calm water resistance, sinkage and trim at $Fr = 0.2$ and 0.6, and wave-induced motions in regular head waves with $\lambda/L = 1.63$ at $Fr = 0.6$.

Grid Triplet; r_G	Iterative		C_T			C_p			C_f			C_s			Sinkage			Trim			Wave elevation		
	U_I%S	U_I/ε_{12}	R_G	P_G	U_G%S	R_G	P_G	U_G%S	R_G	P_G	U_G%S	R_G	P_G	U_G%S	R_G	P_G	U_G%S	R_G	P_G	U_G%S	R_G	P_G	U_G%S
Resistance, sinkage and trim at $Fr = 0.2$																							
1,2,3; $2^{1/4}$	0.39	0.17	0.24	1.05	3.43	−0.62	OC	1.24	0.46	1.1	5.4	0.6	0.75	7.06	0.21	2.25	6.29	−1.44	OD	–	~0.5	~0.9	~15
1,3,5; $2^{1/2}$			−3.13	OD	–	−0.4	OC	1.86	2.71	MD	–	−2	OD	–	0.52	0.9	6.4	0.875	0.2	20.1			
Resistance, sinkage and trim at $Fr = 0.6$																							
1,2,3; $2^{1/4}$	0.12	0.06	0.33	0.8	0.77	0.24	2.1	3.29	0.43	1.2	4.90	−0.8	OC	0.16	−0.23	OC	3.04	0.05	3.5	2.06	0.4	0.75	3.8
1,3,5; $2^{1/2}$			−0.67	OC	0.36	−0.51	OC	3.65	−0.25	OC	1.02	0.2	2.0	5.42	−0.21	OC	5.91	2.75	MD	–			

	Iterative		C_T			Pitch time history			Heave time history			z_1/A			θ_1/Ak			Heave phase			Pitch phase		
	U_I%S	U_I/ε_{12}	R_G	P_G	U_G%S	R_G	P_G	U_G%S	R_G	P_G	U_G%S	R_G	P_G	U_G%S	R_G	P_G	U_G%S	R_G	P_G	U_G%S	R_G	P_G	U_G%S
Seakeeping, $Fr = 0.6$, $\lambda/L = 1.63$																							
1,2,3; $2^{1/4}$	0.08	0.03	0.8	0.32	5.88	−0.35	OC	3.50	0.1	2.5	3.80	0.80	0.32	4.53	0.74	0.43	6.33	−0.94	OC	4.0	0.46	1.1	2.39
1,3,5; $2^{1/2}$			0.66	0.6	3.40	0.23	1.4	3.80	0.26	1.6	2.60	0.60	0.7	2.03	0.49	1.03	4.9	0.65	0.31	2.40	0.54	0.95	0.46

MD: Monotonic Divergence; OD: Oscillatory Divergence; OC: Oscillatory convergence.
R_G: Convergence ratio.
P_G: Ratio of predicted and theoretical numerical order of accuracy.

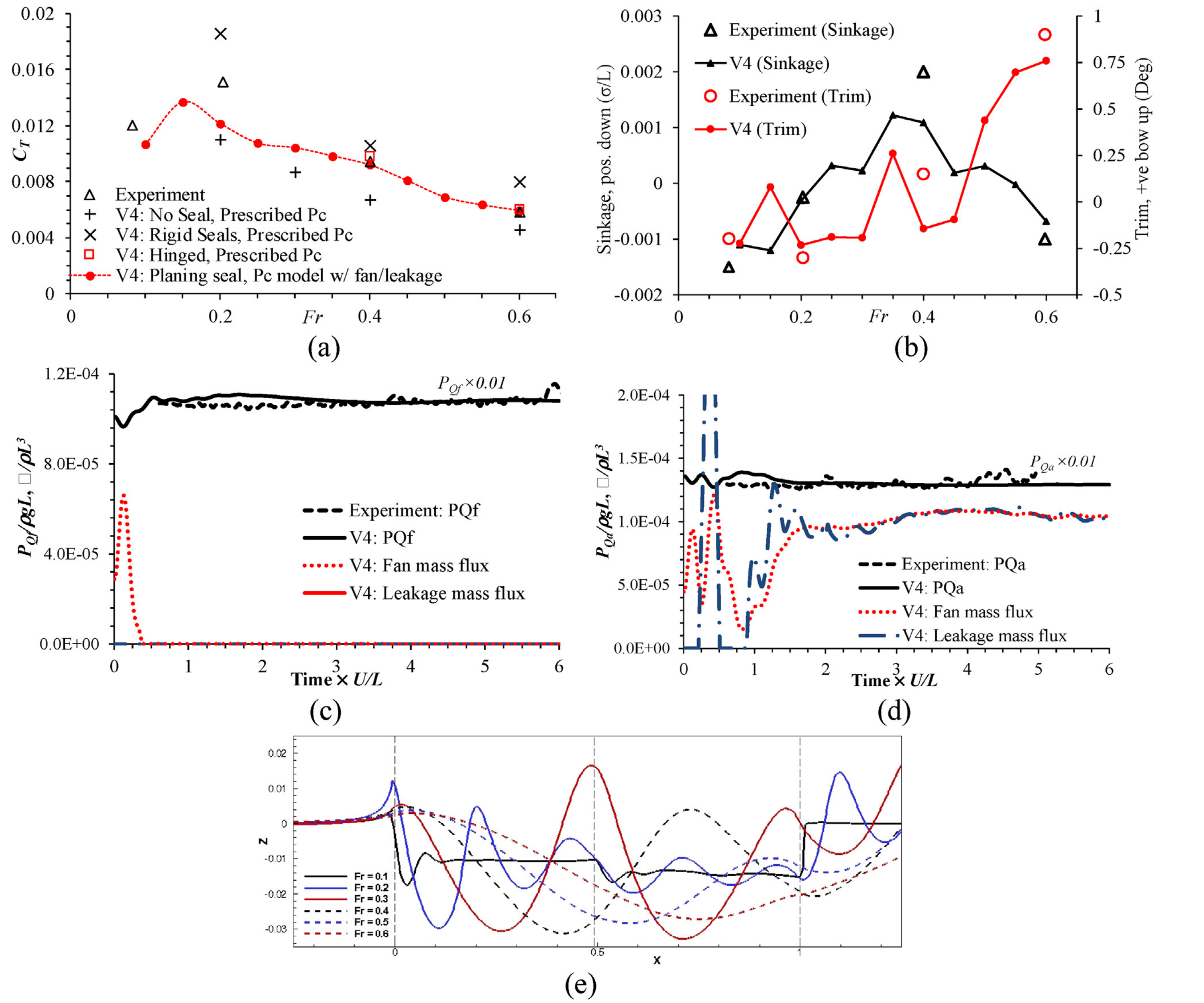

Fig. 3. Calm water resistance, sinkage, trim and air cushion pressure predictions are compared with experimental data [16]. (a) C_T predicted using different seal models. (b) Sinkage and trim predictions. (c) Forward air cushion pressure, fan and leakage mass flux, and (d) aft air cushion pressure, fan and leakage mass flux at $Fr = 0.4$. (e) Center-line wave elevation for different Fr.

Table 4
Numerical order of accuracy ratio (P_G), grid uncertainty (U_G) and prediction errors obtained in the simulations are compared with available SES, semi-planing, displacement and high speed planing hull studies.

Case	Grid, Re (Fr)	Calm water resistance			Calm water motions			Wave-induced motions		
		P_G	$U_G\%S$	$\overline{\lvert E\rvert}^{a}\%D$	P_G	$U_G\%S$	$\overline{\lvert E\rvert}\%DR$	P_G	$U_G\%S$	$\overline{\lvert E\rvert}\%DR$
T-Craft (this study)	10 M, 7×10^6 (0.1–0.6)	1.4	*3.8*	**8.1**	2.3	*8.5*	**10.24**	2.14	*4.1*	**13.5**
T-Craft [9]	7×10^6 (0.1–0.6)				**21.6**					
JJMA [7]	4.7 M, 2.6×10^7 (0.2–0.6)		**21.75**							
Displacement hull [23]	9 M, 1.2×10^7 (0.25–0.8)	1.45	*5.9*	**4.22**	1.2	*11.1*	**7.8**			
Semi-planing hull [24]	30 M, 2.6×10^7 (0.15–0.62)	1.17	*1.0*	**3.36**	1.02	*1.2*	**6.65**			
High speed planing hull [27]	14.5 M, 1.6×10^7 (0.6–1.8)		**12.3**		**11.9**		**18.4**			

[a] $\overline{|E|} = \frac{1}{N}\sum |E|$, where N is number of samples.

for both the SES, $C_{\zeta c}$ predictions agree qualitatively well with the ACV $C_{\zeta c}$ predictions, with maxima at $Fr = 0.3$ and 0.6, and minima around $Fr = 0.4$. Note that JJMA predictions show large $C_{\zeta c}$ values for $Fr = 0.3$ consistent with ACV simulations with sharp edged air cushion pressure patch. Whereas T-Craft predictions compare well with ACV simulations with the smooth edged air cushion pressure patch. The results are consistent with the air cushion modeling used in the respective studies. Experimental data for JJMA in Fig. 4(b) shows that the resistance decreases with the increase in Fr, similar to T-Craft, but shows 30–40% higher values. Figs. 4(c) and (d) show the C_T components for T-Craft and JJMA, respectively. For T-Craft, averaged C_p, C_f, C_s, C_{ac} and C_A contributions are 43.5%, 22%, 32%, 1.7% and 1%C_T, respectively. The corresponding contributions for JJMA are 23.6%, 26%, 28%, 22% and 2.8%C_T, respectively. Both SES

Table 5
Summary of comparison errors in calm water, impulsive motions and wave-induced motion cases.

Case	Models	*Fr*	*C_T (E%D)*					
			P_{0i} No Seal	P_{0i} Rigid Seal	P_{0i} Hinged Seal	P_{0i} 2D planing surface seal	P_i 2D planing surface seal	P_{Qi} 2D planing surface seal
Calm water Resistance *(Compare air cushion and seal models)*	Different seal and air cushion models	0.2	27.45	−22.53	–	17.77	17.28	18.85
		0.4	29.09	−11.98	−3.44	10.07	5.04	−0.39
		0.6	21.46	−36.85	−2.34	9.30	−2.21	4.36
		$\overline{\lvert E\rvert}$	*26.0*	*23.79*	*2.89*	*12.37*	*8.18*	*7.87*

Case	Models	*Fr*	C_T	Sinkage		Trim		P_{Qf} (E%D)	P_{Qa} (E%D)
			(E%D)	E%D	E%DR	E%D	E%DR		
Calm water resistance, sinkage and trim (Validation)	P_{Qi}, 2D planing surface seal	0.1	8.53	26.67	11.43	−13.43	−2.21	−2.45	10.95
		0.2	18.85	−25.2	−1.8	22.65	5.66	−2.97	13.93
		0.4	−0.39	−45.5	−26	195.5	−24.45	−1.21	4.29
		0.6	4.36	31.7	9.06	15.61	−11.71	0.9462	−4.09
		$\overline{\lvert E\rvert}$	8.03	32.26	12.1	61.8	11	1.89	8.32

Case	Models	Variables	Heave (E%D)				Pitch (E%D)			
			P_A	P_{0i}	P_i	P_{Qi}	P_A	P_{0i}	P_i	P_{Qi}
Impulsive motions *(Compare air cushion models and Validation)*	Different air cushion models, 2D planing surface seal	f_n	1.72	6.2	4.44	1.83	0.25	7.0	5.01	2.03
		Amplitude	6.82	38.26	12.30	9.21	2.02	60.7	8.46	4.60
		P_{Qf}	–	–	−35.7	−8.03	–		−24.81	−22.44
		P_{Qa}	–	–	−18.6	−2.87	–		−30.8	−22.05
		$\overline{\lvert E\rvert}$	*4.27*	*22.23*	*17.26*	*5.48*	*1.14*	*33.85*	*17.27*	*12.78*

Case (Models)		Variables	$\overline{\lvert E\rvert}$[a]				
			C_T (%D)	Pitch (%DR)	Heave (%DR)	P_{Qf} (%D)	P_{Qa} (%D)
Wave-induced motions P_{Qi}, 2D planing surface seal (Validation)	Regular head waves $\mu = 0^\circ$, $Fr = 0$	0th Harmonic				6.25	3.86
		1st Harmonic		18.75	32.59	5.79	6.97
		Phase		2.21	1.67		
	Regular head waves $\mu = 0^\circ$, $Fr = 0.6$	0th Harmonic	7.51	10.67	17.81	7.1	1.96
		1st Harmonic	35.61	22.42	21.9	15.82	4.56
		Phase		3.81	3.03		
	$\overline{\lvert E\rvert}$		21.56	11.57	15.4	7.03	

[a] Error averaged over λ/L range.

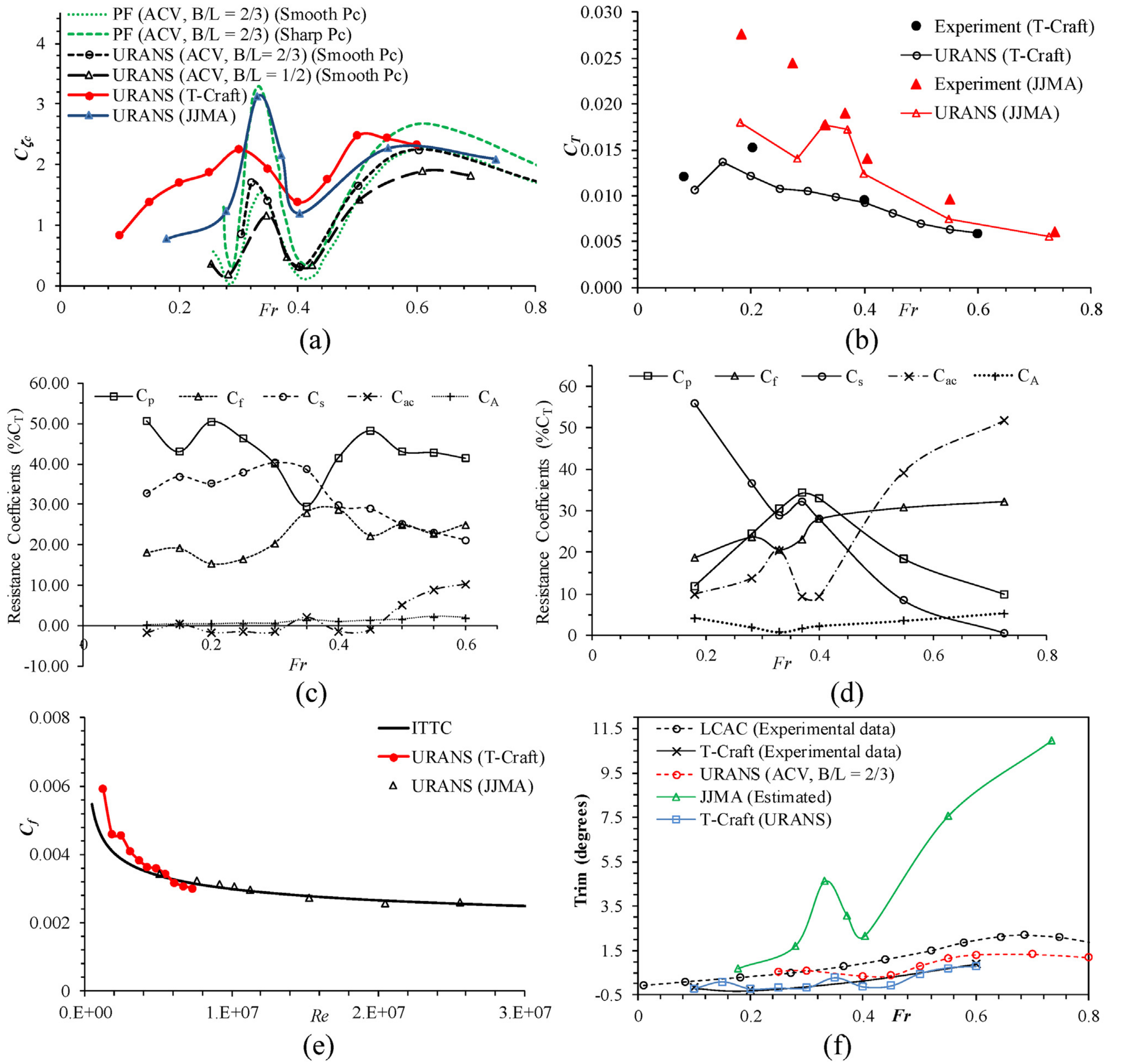

Fig. 4. (a) T-Craft $C_{\zeta c}$ predictions (refer to Bhushan et al. [3] for non-dimensionalization) are compared with URANS and PF predictions for ACV, and URANS predictions for JJMA. (b) Comparison of T-Craft and JJMA calm water resistance. Components of the resistance coefficients obtained for (c) T-Craft, and (d) JJMA reported by [7]. (e) C_f predictions (based on dynamic wetted are) for T-Craft and JJMA are compared with ITTC correlation $C_{f,ITTC} = 0.075/(log_{10}Re - 2)^2$. (f) Trim reported by LCAC ACV and T-Craft experiments, are compared with URANS predictions for ACV [3], T-Craft, and JJMA (estimated in this study).

show similar C_f, C_s and C_A contributions. For both, C_f predictions compare well with ITTC correlation (Fig. 4e), and C_A contributions are small. However, they show significant differences in the C_p and C_{ac} contributions. T-Craft predictions show 2 times higher C_p contributions than those for JJMA. T-Craft predictions show small C_{ac} contribution, which varies from <1%C_T (or 5%$C_{\zeta c}$) for lower Fr to around 10%C_T (or 40%$C_{\zeta c}$) for $Fr > 0.5$. An analysis of the ACV results [3] using Eq. (3) suggests $C_{ac} \sim 10\%C_{\zeta c}$ for $Fr = 0.3$ to 0.8, which is in good agreement with T-Craft predictions. JJMA predictions show significantly large C_{ac} which varies from 10%C_T for $Fr = 0.2$ to around 40–50%C_T for $Fr \geq 0.55$. The JJMA study did not report trim predictions; however using Eq. (3), the trim is estimated to be $\tau \sim 8°–11°$ for $Fr \geq 0.55$ (Fig. 4f). Experimental data is not available to ascertain whether the estimated trim values are plausible. However, they are significantly large compared to the available ACV and SES experimental data [16,25] and URANS results [3]. Overall, there is a discrepancy in the T-Craft and JJMA estimates for C_{ac}, which could be due to the equilibrium assumption in the air cushion used by [7], and needs to be further investigated.

6. Impulsive motions

Table 4 and Fig. 5 summarize the impulsive heave and pitch simulation results. Experimental data for catamaran operation show that heave and pitch natural frequencies are within 2.5% of each other, consistent with Delft catamaran [26] study. For SES operation, the heave natural frequency is 13% larger than that for the pitch.

Preliminary studies compare P_{0i}, P_i and P_{Qi} air cushion models. The errors are smallest for P_{Qi} air cushion model, as was also the case for calm water resistance. Thus, only P_{Qi} results are discussed hereafter. URANS predictions for the catamaran operation compare

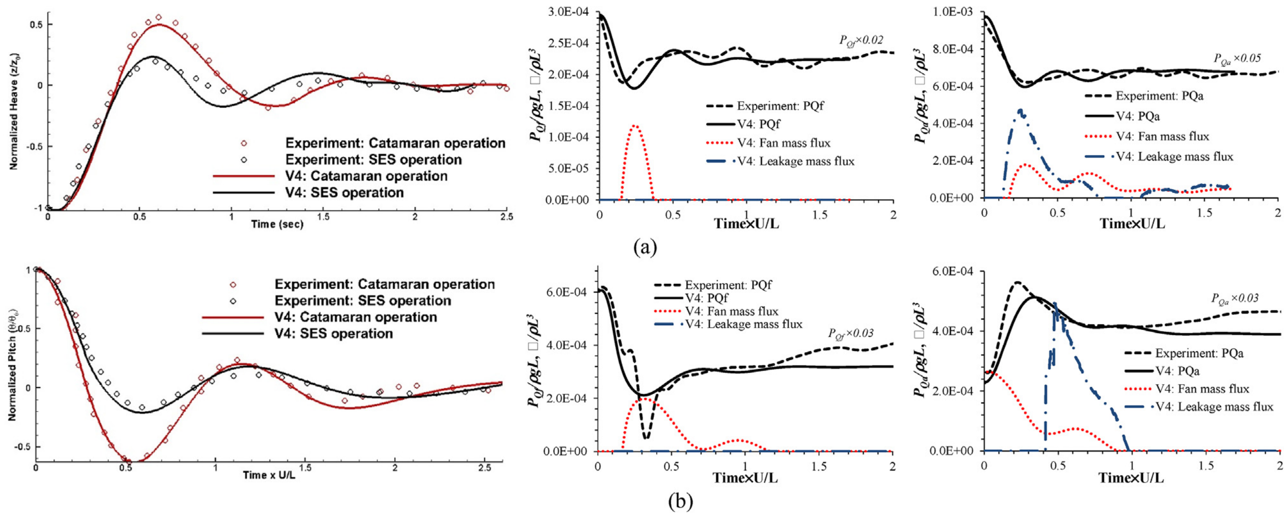

Fig. 5. URANS predictions of the time history of the motions (LEFT), forward air cushion pressure (MIDDLE) and aft air cushion pressure (RIGHT) for catamaran and SES operations are compared with experimental data for impulsive (a) heave and (b) pitch cases.

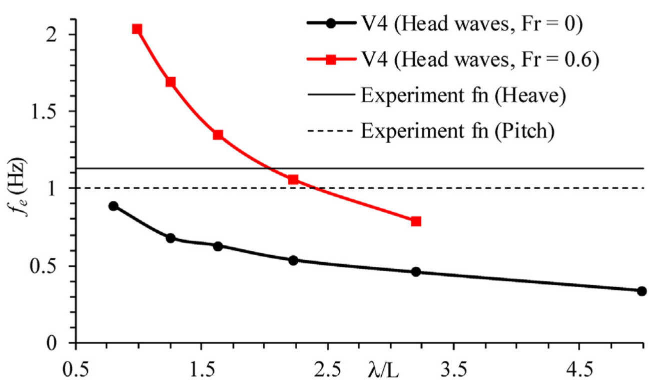

Fig. 6. Encounter frequency vs λ/L for wave-induced motion predictions in regular head waves at $Fr = 0$ and 0.6 are compared with experimental heave and pitch natural frequencies.

within 4.3%D and 1.2%D of the experiments for heave and pitch, respectively. For the SES operation, heave and pitch errors compare reasonably well, with averaged errors of 5.5%D and 12.8%D, respectively. The errors are smallest to largest for the prediction of natural frequencies, amplitudes and air cushion pressures.

7. Resistance and wave-induced motions in head waves at *Fr* = 0 and 0.6

Fig. 6 shows encounter frequency $f_e = U_0\left[\frac{1}{Fr\sqrt{2\pi\lambda L}} + \frac{1}{\lambda}\cos(\mu)\right]$ vs. λ/L for each Fr, including horizontal lines marking experimental heave and pitch natural frequencies. The heave/pitch resonance occur near $\lambda/L = 0.5$ and 2 at Fr=0 and 0.6, respectively.

The 1st harmonic of the resistance, motions and air cushion pressures are shown in Fig. 7, and comparison errors are summarized in Table 4. Experiments at $Fr = 0$ show small heave and pitch response for shorter wavelengths, a peak at $\lambda/L = 1.5$ followed by overshoot at $\lambda/L = 3.25$, and approach unity for longer wavelengths as expected for λ » beam (B). Experiments at $Fr = 0.6$ are very limited, i.e., for only three $\lambda/L < 2$, thus it is hard to identify any trends. However, the data for $\lambda/L = 1.63$ seem outliers.

URANS predictions agree with most of the experimental trends at $Fr = 0$, but show large error of 23%DR for motion amplitudes. The motion amplitudes are small for smaller λ/L, thus dynamic range is used for the% calculation. The motion phases are predicted well within 2.7%DR of the experiments. The air cushion pressure predictions show reasonable agreement with the experimental data for which the averaged error is 7.6%D. The resistance predictions at $Fr = 0.6$ agree very well with the experiments for the two smaller λ/L, but show large error for $\lambda/L = 1.63$. The predictions for $\lambda/L > 2$ show asymptotic behavior, as expected.

The 0th harmonic of the resistance, motions and air cushion pressures, including added resistance, are shown in Fig. 8. Experimental data show that the heave and pitch are close to zero at $Fr = 0$, and close to the calm water values at $Fr = 0.6$, except for the sharp change at $\lambda/L = 1.63$. The air cushion pressures are mostly close to the initial air cushion pressure. The added resistance ΔC_T is almost the same for the two smaller λ/L, at about 10% of calm water C_T. However for $\lambda/L = 1.63$, ΔC_T shows a sudden drop and is negative, which is unexpected.

The URANS predictions overall agree well with the experimental trends. The averaged errors for C_T, z, θ, ϕ and P_{Qi} are 21.6%D, 15.4%D, 11.6%DR, 22%DR and 7%D, respectively. The added resistance predictions are almost similar for the entire λ/L, and compare within 7.5%D of the experiments for the two smaller λ/L.

8. Conclusions

SES air cushion and seal models are implemented in a URANS hydrodynamics solver. Air cushion is modeled either as a prescribed pressure patch, or as a compressible isothermal/adiabatic ideal stagnant air with fan and leakage flows. Seal modeling includes discretized rigid and hinged bow and stern seals, and 2D planing surface bow seal with hydrodynamic interaction. The models are assessed based on verification and validation studies using T-Craft experimental data for calm water resistance, sinkage and trim at $Fr = 0.1$–0.6; impulsive heave and pitch at $Fr = 0$; and wave-induced resistance and pitch and heave in regular head waves at $Fr = 0$ and 0.6. The compressible air cushion model with fan and leakage flows perform better than that without the fan and leakage flows and the prescribed pressure patch model for motion predictions. The hinged seal model performs better than the 2D planing surface seal and rigid models for resistance predictions, but is computationally expensive for time-accurate simulations. Therefore, the next best option, i.e., the 2D planing surface seal model, is used in the validation study.

Grid verification shows averaged grid uncertainty of 2%, 8% and 10% for resistance, motions and wave-elevation, respectively, on

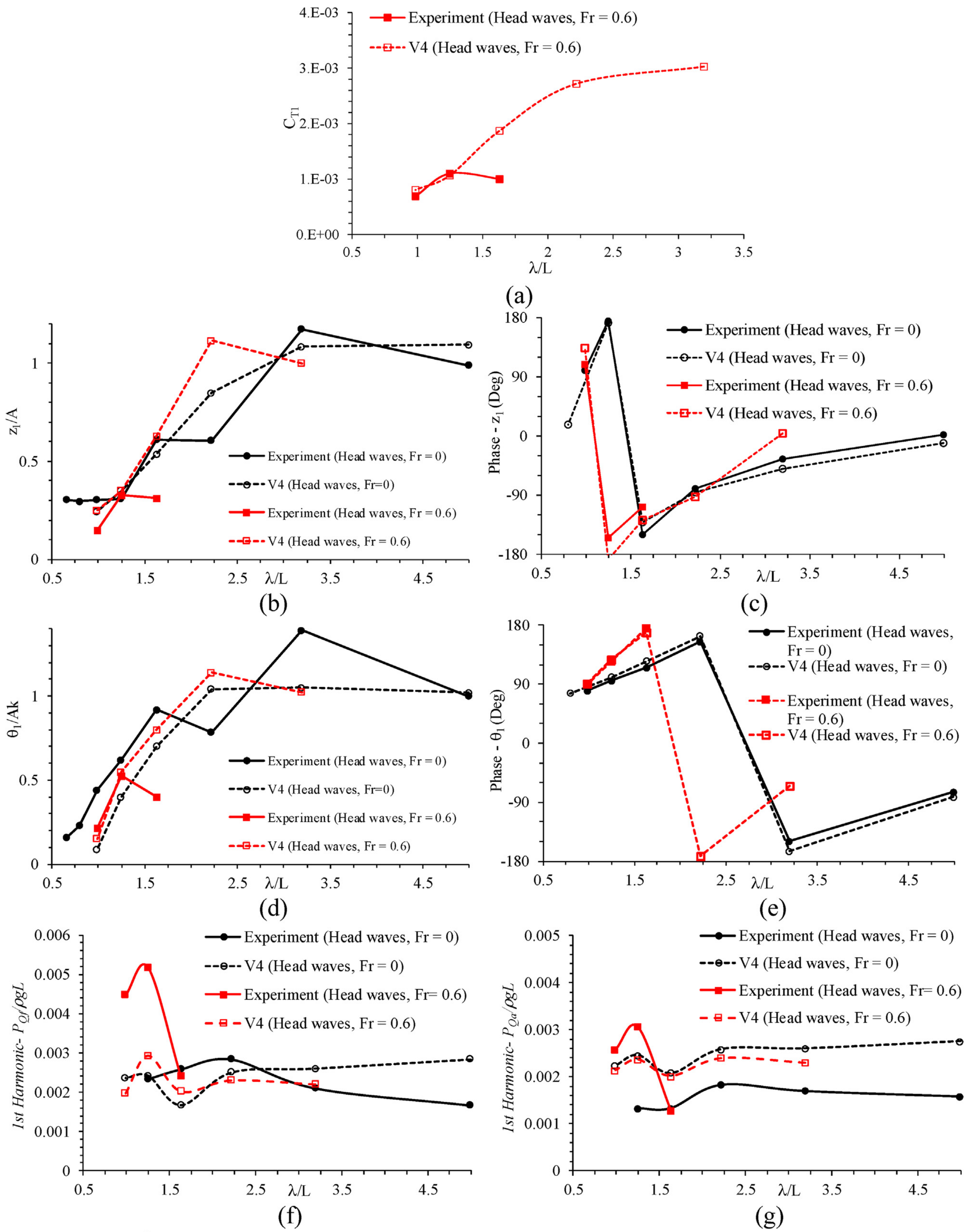

Fig. 7. 1st harmonic predictions for wave-induced motions in regular head waves at $Fr = 0$ and 0.6 are compared with experimental data [16]. (a) Resistance; heave (b) amplitude and (c) phase; pitch (d) amplitude and (e) phase; (f) forward and (g) aft air cushion pressures.

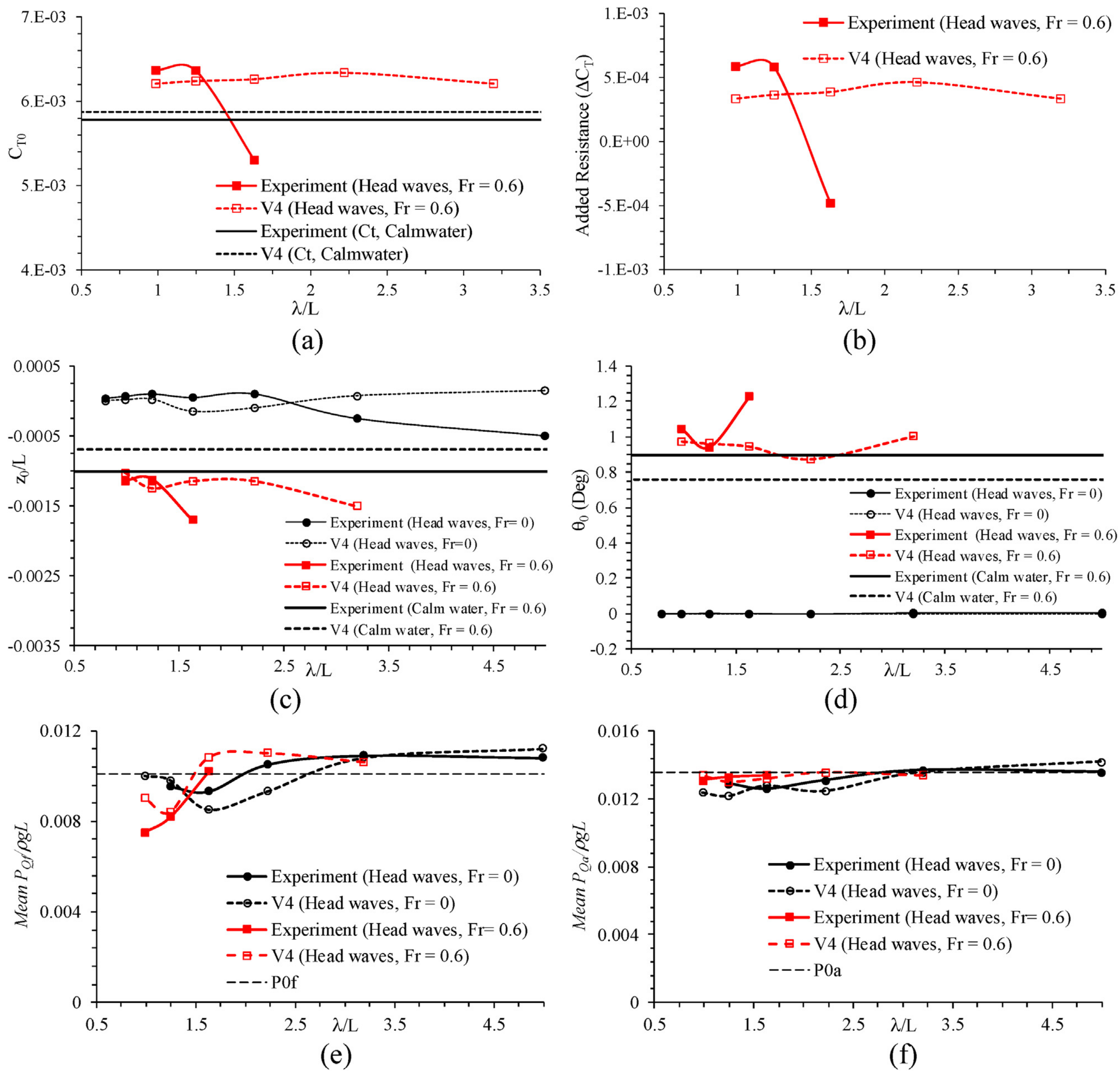

Fig. 8. 0th harmonic predictions for wave-induced motions in regular head waves at $Fr = 0$ and 0.6 are compared with the experimental data [16]. (a) Mean and (b) added resistance at $Fr = 0.6$; (c) mean heave; (d) mean pitch; and (e) forward and (f) aft air cushion pressures.

grids consisting of 5.2 M cells. The grid uncertainties are reasonable and comparable to semi-planing and displacement hull studies on similar size grids.

T-Craft resistance is primarily due to C_p, C_s and C_f, which accounts for about 45%, 30% and 20%C_T, respectively. C_{ac} contribution varies from 1% to 10%C_T, and C_A contributions are <1%C_T. The T-Craft and JJMA [7] predictions are consistent for C_f, C_s and C_A contributions, but show significant differences for C_{ac} contributions. JJMA predictions show C_{ac} up to 50%C_T, which suggests that it has an order of magnitude larger trim than ACVs and T-Craft. Both SES have similar air cushion dimensions and pressures, thus the differences in C_{ac} contribution are probably due to the differences in the calculation approach. Herein, C_{ac} is calculated from surface pressure integration, whereas it was estimated assuming equilibrium condition in the air cushion in [7]. Overall, the present study does not support the estimation of C_{ac} using equilibrium assumption, and the validity of the assumption needs further investigation.

Calm water resistance and motions, impulsive heave and pitch, and associated air cushion pressure predictions compare within 8.5% of the experimental data. The resistance predictions are significantly better than the SES study [7], and the resistance and motion predictions are comparable to the displacement, semi-planing and high speed planing hull studies [23,24,27] as summarized in Table 4. The wave-induced motion predictions follow the experimental trends, but show relatively larger errors around 13.5%. Nevertheless, the prediction errors are lower than those reported by the T-Craft study [9], and are comparable to those of high speed planing hull study [24].

The air cushion and especially seal models implemented in the URANS solver are very approximate, but are able to predict the experimental trends well and the prediction errors are reasonable. However, they show some deficiencies, e.g., they fail to predict the sharp peaks and troughs in aft and forward air cushion pressures, respectively. The most critical advancements needed for future studies are for the seal modeling, including extension of the 2D planing seal model to 3D, ability to account for the effect of roll, and in the long run develop a robust model using fluid structure interactions.

Acknowledgements

The Office of Naval Research under Grant N00014-10-1-0499 administered by Ms. Kelly Cooper sponsored this research. Prof. Lawrence J. Doctors from The University of New South Wales, Sydney, Australia provided Potential flow results for the 2D planing surface bow seal model.

References

[1] L.J. Doctors, Representation of planing surfaces by finite pressure element, Proc. Fifth Australian Conference on Hydraulics and Fluid Mechanics 2 (1974) 480–488.
[2] L.J. Doctors, V. Tredge, C. Jiang, C.B. Mckesson, Optimization of a split-Cushion surface-Effect ship, in: Proceedings of 8th International Conference on Fast Sea Transportation, Russia, 2005.
[3] S. Bhushan, F. Stern, L.J. Doctors, Verification and validation of URANS wave resistance for air cushion vehicles, and comparison with linear theory, J. Ship Res. 55 (4) (2011) 249–267.
[4] K.J. Maki, R. Broglia, L.J. Doctors, D. Mascio, Nonlinear wave resistance of a two-dimensional pressure patch moving on a free surface, Ocean Eng. 39 (2012) 62–71.
[5] L.J. Doctors, Near-field hydrodynamics of a surface-effect ship, J. Ship Res. 56 (3) (2012) 183–196.
[6] C.B. Mckesson, L.J. Doctors, Scaling of resistance from surface-effect ship model tests, in: Proc. 11th International Conference Fast Sea Transportation, Hawaii, USA, 2011.
[7] K.J. Maki, R. Broglia, L.J. Doctors, A. DiMascio, Numerical investigation of the components of calm-water resistance of a surface-effect ship, Ocean Eng. 72 (2013) 375–385.
[8] W.H. Milewski, B. Connell, B. Petersen, Initial validation of the ACVSIM model for dynamics of air cushion vehicles, in: 27th Symposium on Naval Hydrodynamics, Seoul Korea, 2008.
[9] B. Connell, W.H. Milewski, B. Goldman, D. Kring, Single and multi-Body surface effect ship simulation for T-Craft design evaluation, in: Proc. 11th International Conference Fast Sea Transportation, Hawaii, USA, 2011.
[10] J.C. Bandas, J.M. Falzarano, JA numerical investigation into the linear seakeeping ability of the T-Craft, in: Proc. 11th International Conference Fast Sea Transportation, Hawaii, USA, 2011.
[11] C.-H. Lee, J.N. Newman, Wave effects on large floating structures with air cushions, Mar. struct. 13 (2000) 315–330.
[12] A. Mouravieff, A CFD-Based Analysis of Surface Effect Ship Hydrodynamics, Stevens Institute of Technology, USA, 2010, Master Thesis.
[13] D. Donnelly, W.L. Neu, Numerical simulation of flow about a surface-effect ship, in: Proc. 11th International Conference Fast Sea Transportation, Hawaii, USA, 2011.
[14] S. Bhushan, P.M. Carrica, J. Yang, F. Stern, Scalability and validation study for large scale surface combatant computations using CFDShip-Iowa, Int. J. High Perform. Comput. Appl. 25 (4) (2011) 466–487.
[15] F. Stern, et al., Recent progress in CFD for naval architecture and ocean engineering, J. Hydrodyn. Ser. B 27 (1) (2015) 1–23.
[16] R.C. Bishop, A.L. Silver, D. Tahmasian, S.S. Lee, J.L. Park, L.A. Snyder, J. Kim, T-Craft Seabase Seakeeping Model Test Data Report, Naval Surface Warfare Center Carderock Division, 2009, Technical Report, NSWCCD-50-TR–2009/055.
[17] O.M. Faltinsen, Hydrodynamics of High-speed Marine Vehicles, 1st edition, Cambridge University Press, 2005, pp. 141–163.
[18] A.H. Day, D. Clelland, L.J. Doctors, P. Beveridge, Resistance of a compartmented surface-Effect ship, J. Prod. Des. 26 (3) (2010) 219–230.
[19] A. Malakhoff, S. Davis, Evolution of surface effect ship (SES) bow seals, in: 19th Annual Technical Symposium, Association of Scientist and Engineers of the Naval Sea Systems Command, Washington, DC, 1982.
[20] F. Stern, R. Wilson, J. Shao, Quantitative approach to V&V of CFD simulations and certification of CFD codes, Int. J. Numer. Methods Fluids 50 (2006) 1335–1355.
[21] T. Xing, F. Stern, Factors of safety for richardson extrapolation, Trans. ASME J. Fluids Eng. 132 (6) (2010) 061403.
[22] F. Ismail, P.M. Carrica, T. Xing, F. Stern, Evaluation of linear and nonlinear convection schemes on multidimensional non-orthogonal grids with applications to KVLCC2 tanker, Int. J. Numer. Meth. Fluids 64 (2010) 850–886.
[23] S. Bhushan, T. Xing, F. Stern, Vortical structures and Instability analysis for Athena wetted transom flow with full-scale validation, J. Fluids Eng. 134 (2012) 031201.
[24] E. Lee, A. Fullerton, J. Geiser, C. Schleicher, C. Merrill, C. Weil, M. Jiang, V. Lien, J. Morin, F. Stern, M. Mousaviraad, Experimental and computational comparisons of the R/V athena in calm water, in: 31st Symposium on Naval Hydrodynamics Monterey, CA, USA, 11–16 September, 2016.
[25] J.J. Ricci, A.J. Becnel, M.L. Butler, J.G. Hoyt III, L.A. Snyder, Towing Tank Report on a Comparative Study of Four LCAC Skirt Systems, Naval Systems Warfare Center, Panama City Division, 2008, Report NSWC PCD/TN-E32-08/014, June.
[26] T. Castiglione, F. Stern, S. Bova, M. Kandasamy, Numerical investigation of the seakeeping behavior of a catamaran advancing in regular head waves, Ocean Eng. 38 (16) (2011) 1806–1822.
[27] T.C. Fu, K.A. Brucker, S.M. Mousaviraad, C.M. Ikeda, E.J. Lee, T.T. O'Shea, Z. Wang, F. Stern, C.Q. Judge, An assessment of computational fluid dynamics predictions of the hydrodynamics of high-speed planing craft in calm water and waves, in: Proc. 30th Symposium on Naval Hydrodynamics, Hobart, Tasmania, Australia, November 2–7, 2014.